

Deformation Mechanisms During Intermediate-Temperature Steady-State Creep in Nickel-Based Single Crystal Superalloys: Postprint

Authors: Su Yong, Tian Sugui, Yu Huichen, Yu Lili

Date: 2023-03-19T00:00:00+00:00

Abstract

Through creep property testing, microstructural morphology observation, and diffraction contrast analysis of dislocation configurations, the deformation mechanisms of nickel-based single crystal superalloys during medium-temperature/high-stress steady-state creep were investigated. The results indicate that during creep at 760 °C, 760 MPa and 800 °C, 650 MPa, dislocations shearing the γ phase can dissociate; following dissociation, the leading $a/3\langle 112 \rangle$ superlattice Shockley partial dislocation cuts into the γ phase, while the trailing $a/6\langle 112 \rangle$ Shockley partial dislocation remains at the γ/γ phase interface, forming a superlattice intrinsic stacking fault (SISF) between the two partial dislocations. Additionally, superlattice dislocations shearing into the γ phase can cross-slip from the $\{111\}$ plane to the $\{100\}$ plane, forming Kear-Wilford (K-W) locks with non-planar dislocation core structures, which can suppress dislocation slip and cross-slip, thereby enhancing the alloy's creep resistance. During creep at 850 °C, 500 MPa, stacking faults in the alloy disappear; some $a\langle 110 \rangle$ superlattice dislocations shearing into the rafted γ phase can dissociate to form a configuration of “two $a/2\langle 110 \rangle$ partial dislocations plus an anti-phase boundary (APB)”, while the disappearance of K-W locks in the alloy is caused by high-temperature thermal activation inducing cross-slip of dislocations from cube slip back to octahedral planes.

Full Text

Acta Metallurgica Sinica, Vol. 51, No. 12, December 2015, pp. 1472-1480

Deformation Mechanisms of Ni-Based Single Crystal Superalloys During Steady-State Creep at Intermediate Temperatures

SU Yong^{1,2}), TIAN Sugui¹), YU Huichen³), YU Lili¹)

¹⁾ School of Materials Science and Engineering, Shenyang University of Technology, Shenyang 110870

²⁾ School of Energy and Power Engineering, Shenyang University of Chemical Technology, Shenyang 110142

³⁾ Science and Technology on Advanced High Temperature Structural Materials Laboratory, Beijing Key Laboratory of Aeronautical Materials Testing and Evaluation, AVIC Beijing Institute of Aeronautical Materials, Beijing

Abstract

Through creep performance testing, microstructural observation, and diffraction contrast analysis of dislocation configurations, the deformation mechanisms of a Ni-based single crystal superalloy during steady-state creep at intermediate temperatures and high stresses were investigated. The results show that during creep at 760 °C/760 MPa and 800 °C/650 MPa, dislocations shearing the γ phase can decompose. Leading $a/3$ 112 superlattice Shockley partial dislocations cut into the γ precipitates while trailing $a/6$ 112 Shockley partial dislocations remain at the γ/γ interface, forming superlattice intrinsic stacking faults (SISF) between the two partial dislocations. Additionally, superdislocations shearing into the γ phase can cross-slip from $\{111\}$ to $\{100\}$ planes, forming Kear-Wilford (K-W) locks with non-planar dislocation core structures that inhibit dislocation slip and cross-slip, thereby enhancing creep resistance. During creep at 850 °C/500 MPa, stacking faults disappear in the alloy, and some $a/110$ superdislocations shearing into the rafted γ phase decompose into configurations of “two $a/2$ 110 partial dislocations plus antiphase boundary (APB).” The disappearance of K-W locks at this temperature results from thermal activation at high temperatures causing dislocations on cube slip planes to cross-slip back onto octahedral planes.

Keywords: Ni-based single crystal superalloy; creep; dislocation; stacking fault; deformation mechanism

1. Introduction

γ/γ two-phase Ni-based single crystal superalloys exhibit excellent high-temperature mechanical properties and creep resistance, making them widely used as turbine blade materials in gas turbines and aero-engines [1-3]. Under centrifugal forces during high-temperature service, creep damage remains the primary failure mode for these alloys [4-6], with dislocations cutting into the γ strengthening phase and subsequent crack initiation and propagation at γ/γ interfaces representing important causes of late-stage creep failure [7].

Single crystal blade components experience multiple cycles of varying conditions, including intermediate temperature/high stress and high temperature/low stress regimes during service. Internal air-cooling of blades can reduce the actual service temperature below that of the engine hot section [8], making system-

atic investigation of creep behavior at intermediate temperatures (750–850 °C) and high stresses crucial. It is generally accepted that during intermediate-temperature creep, dislocations cutting into the γ phase form configurations of “partial dislocations plus stacking faults” (intrinsic stacking faults (SISF), extrinsic stacking faults (SESF), or complex faults (CF)) [9–12]. The stacking fault energy influences the ease of partial dislocation constriction and thus affects strengthening effectiveness [13]. Studies show that stacking faults disappear when applied stress is below 500 MPa [14,15] or temperature exceeds 950 °C [16], while “partial dislocations plus antiphase boundary (APB)” configurations appear within rafted γ phases under high-temperature service conditions [7].

Although literature has reported dislocations shearing into γ phase forming “partial dislocations plus SISF or APB” configurations, different viewpoints persist regarding the decomposition mechanisms [17–19]. For instance, during steady-state creep of CMSX-2 single crystal alloy at 760 °C/750 MPa, $a/2$ 110 partial dislocations (where a is the lattice constant) existed within the γ phase [17], whereas under identical conditions, IP René 80 alloy formed “ $a/3$ 112 partial dislocations plus stacking fault” configurations [18]. During steady-state creep of Ni-based single crystal alloys at 760 °C/780 MPa, stacking faults formed with $a/3$ 112 and $a/6$ 112 partial dislocations located within the γ phase and at γ/γ interfaces, respectively [19]. These findings demonstrate that different single crystal alloys exhibit distinct dislocation shearing modes and characteristics even under similar creep conditions. Since intermediate-temperature creep behavior and γ phase deformation mechanisms directly affect the reliability of engine blade components, systematic investigation of these phenomena is essential.

This work examines the creep behavior and dislocation shearing characteristics of a [001]-oriented Ni-based single crystal superalloy under conditions of 760 °C/760 MPa, 800 °C/650 MPa, and 850 °C/500 MPa through creep testing, microstructural observation, and dislocation configuration analysis to refine intermediate-temperature creep theory for Ni-based single crystal superalloys.

2. Experimental Methods

A master alloy with composition Ni-9.0Cr-5.0W-5.5Al-4.5Co-1.7Ti (wt.%) was directionally solidified into [001]-oriented single crystal bars using a high-temperature gradient vacuum furnace with grain selection. Laue back-reflection diffraction confirmed the crystal orientation, revealing angular deviations of 7°, 26°, and 22° from the [001], [113], and [012] directions, respectively. The alloy underwent heat treatment of 1250 °C for 4 h, air-cooled (A.C.), followed by 870 °C for 32 h, A.C. Heat-treated specimens were mechanically ground, polished, and chemically etched using a solution of 100 mL HCl + 80 mL H₂O + 20 g CuSO₄. Microstructural observation on various crystal planes was performed using an S-3400N scanning electron microscope (SEM) to characterize the three-dimensional microstructure.

Creep specimens with a gauge section of 4.5 mm \times 2.5 mm and gauge length of 20.0 mm were machined along (100), (001), and (010) planes, with the broad surface being the (100) plane. After surface grinding and polishing, specimens were tested in a GWT504 high-temperature creep machine at 760 °C/760 MPa, 800 °C/650 MPa, and 850 °C/500 MPa, with creep curves recorded. Tests were terminated at the steady-state stage to preserve dislocation configurations, followed by cooling under load. Thin foils of 3 mm diameter and \sim 50 μ m thickness were prepared and electropolished using a twin-jet apparatus (MTP-1A) at temperatures below -20 °C with an electrolyte of 10% HClO₄ + 90% C₂H₅OH (vol.%). Dislocation configurations were examined using a Tecnai-20 transmission electron microscope (TEM) with double-tilt holder and two-beam technique for diffraction contrast analysis and dislocation line vector determination.

2. Results and Discussion

2.1 Creep Characteristics of the Alloy

The microstructure of the [001]-oriented Ni-based single crystal superalloy after heat treatment is shown in the SEM image of the (100) plane [Figure 1: see original paper]. The γ phase exhibits a cubic morphology with an average edge length of \sim 0.4 μ m, regularly aligned along the [001] and [010] directions. Identical cubic γ morphologies were observed on (001) and (010) planes, confirming that the heat-treated microstructure consists of cubic γ precipitates coherently embedded in the γ matrix and regularly arranged along 100 directions.

Creep curves measured under various intermediate-temperature conditions are presented in [Figure 2: see original paper]. At 760 °C/760 MPa, the alloy exhibited a small initial strain of 1.87% during primary creep, followed by a steady-state stage with a strain rate of 0.0119 %/h lasting \sim 230 h and a total creep life of 379 h. Similar creep characteristics were observed at 800 °C/650 MPa and 850 °C/500 MPa, though with higher steady-state strain rates of \sim 0.0286 %/h and \sim 0.0304 %/h, respectively, and corresponding creep lives of 136 h and 118 h.

2.2 Deformation Characteristics During Steady-State Creep

The TEM micrograph in [Figure 3: see original paper] shows the microstructure after creeping for 40 h at 760 °C/760 MPa (steady-state stage), with the foil normal parallel to [100] and the stress axis indicated by double arrows. After reaching steady-state, the regularly arranged cubic γ precipitates underwent morphological changes, with slight spheroidization of corners and partial diffusion-induced coalescence perpendicular to the stress axis (region I). The γ matrix contained numerous dislocations (regions II and III), with the inset showing local magnification. Some dislocation traces exhibited 90° kinks (arrow 1), attributed to dislocation cross-slip on {111} planes [20]. Additionally, some dislocations sheared into the γ phase (arrow 4). Arrows 2 and 3 indicate mutually perpendicular stacking faults with symmetric dark-bright contrast and

dark outer fringes, identified as SISFs. Partial dislocations bounded these faults [21], with the fault extending ~ 500 nm in width.

TEM images after 40 h at 800 °C/650 MPa and 850 °C/500 MPa are shown in [Figure 4: see original paper]. At 800 °C/650 MPa, cubic γ precipitates further spheroidized and coalesced perpendicular to the stress axis [Figure 4a: see original paper], with some alignment parallel to the stress axis (region IV) possibly related to specimen orientation deviation [22]. Dislocations bowed out in matrix channels (arrows 5 and 6), with limited shearing into γ (arrow 7). Some sheared dislocations decomposed into “partial dislocations plus stacking fault” configurations (arrow 8) with fault width ~ 260 nm. These observations indicate that deformation during steady-state creep at 760 °C and 800 °C involves dislocation slip in the matrix and shearing into γ , with decomposition into “partial dislocations plus stacking fault” configurations.

At 850 °C/500 MPa [Figure 4b: see original paper], local cubic γ transformed into N-type rafts perpendicular to the stress axis. Matrix dislocation density increased significantly, forming high-density interfacial dislocation networks at rafted γ/γ interfaces (region V). Limited dislocations sheared into γ (arrows 9 and 10) without forming stacking fault configurations, indicating deformation mechanisms of matrix slip and γ shearing at 850 °C.

2.3 Diffraction Contrast Analysis of Dislocation Configurations

Dislocation configurations within γ after 40 h at 760 °C/760 MPa are shown in [Figure 5: see original paper], revealing stacking faults (A) bounded by two partial dislocations (C and D) and superdislocations (B) shearing into γ . Using diffraction vectors $g = [002]$, partial dislocations C and D become invisible [Figure 5a: see original paper], while $g = [113]$, $[020]$, and $[133]$ reveal contrast from C [FIGURE:5b-d]. Applying the $b \cdot g = 0$ and $b \cdot g = \pm(2/3)$ invisibility criteria, dislocation C is identified as a superlattice Shockley partial with Burgers vector $b_C = (a/3)[121]$. Dislocation D shows contrast for $g = [113]$ [Figure 5b: see original paper] but disappears for $g = [020]$ and $[133]$ [FIGURE:5c,d], identifying it as a Shockley partial with Burgers vector $b_D = (a/6)[211]$ residing at the γ/γ interface. Using double-tilt to maximize trace length, the line vectors were determined as $\underline{l}_C = [220]$ and $\underline{l}_D = [022]$, establishing the slip plane as $b_C \times \underline{l}_C = b_D \times \underline{l}_D = (111)$. A perpendicular stacking fault (E) indicates at least two equivalent 112 Shockley partial systems decomposing on $\{111\}$ planes. Superdislocation B becomes invisible for $g = [002]$ but visible for $g = [113]$, $[020]$, and $[133]$, identifying it as a perfect superdislocation with Burgers vector $b_B = a[110]$ and line vector $\underline{l}_B = [210]$, giving a slip plane of $b_B \times \underline{l}_B = (100)$.

After 40 h at 800 °C/650 MPa [Figure 6: see original paper], only one orientation of stacking faults (G) exists within γ , bounded by partials H and I, with superdislocation F shearing into γ . Partial H is invisible for $g = [113]$ [Figure 6b: see original paper] but visible for $g = [020]$, $[131]$, and $[131]$ [FIGURE:6a,c,d],

identifying it as a superlattice Shockley partial with $b_{\text{H}} = (a/3)[121]$. Partial I shows contrast for $g = [131]$ [Figure 6d: see original paper] but disappears for $g = [020]$, $[113]$, and $[131]$ [FIGURE:6a-c], establishing it as a Shockley partial with $b_{\text{I}} = (a/6)[211]$ at the γ/γ interface. Superdislocation F is visible for $g = [020]$, $[131]$, and $[131]$ but invisible for $g = [113]$, identifying it as a superdislocation with $b_{\text{F}} = a[110]$. Its maximum length appears parallel to $g = [020]$ [Figure 6a: see original paper], giving line vector $\underline{b}_{\text{F}} = [020]$ and slip plane $b_{\text{F}} \times \underline{b}_{\text{F}} = (001)$.

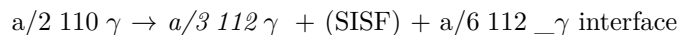
After 40 h at 850 °C/500 MPa [Figure 7: see original paper], γ transformed completely into N-type rafts perpendicular to the stress axis. No stacking fault contrast was observed, though dislocations sheared into the rafted γ (J, K, L). Dislocation K, invisible for $g = [133]$ [Figure 7a: see original paper] but visible for $g = [020]$, $[113]$, and $[022]$ [FIGURE:7b-d], is identified as a perfect superdislocation with $b_{\text{K}} = a[011]$ and line vector $\underline{b}_{\text{K}} = [220]$, slipping on (111). Dislocation L, invisible for $g = [113]$ [Figure 7c: see original paper] but visible for $g = [133]$, $[020]$, and $[022]$ [FIGURE:7a,b,d], is a perfect superdislocation with $b_{\text{L}} = a[110]$ and $\underline{b}_{\text{L}} = [202]$, also slipping on (111). Dislocation J exhibits double-line contrast [Figure 7d: see original paper], decomposing into two partials J1 and J2. Invisible for $g = [020]$ [Figure 7b: see original paper] but visible for $g = [133]$, $[113]$, $[022]$, and $[131]$, both partials have Burgers vectors $b_{\text{J1}} = b_{\text{J2}} = (a/2)[101]$. With line vector $\underline{b}_{\text{J}} = [022]$ [Figure 7d: see original paper], the slip plane is (111). The double-line contrast indicates decomposition into two $a/2$ 110 partials bounding an APB.

3. Analysis and Discussion

3.1 Shearing Behavior of γ Phase

Ni-based single crystal superalloys consist of γ/γ two phases. During initial stages of intermediate-temperature/high-stress creep, deformation occurs by dislocation slip in the matrix. As creep progresses, dislocations become blocked at γ/γ interfaces, pile up, and generate stress concentrations. When the stress peak exceeds the γ yield strength, dislocations shear into γ . Shearing dislocations may decompose on $\{111\}$ into “112 partial dislocations plus SISF” configurations [FIGURE:5 and 6] or form “ $(a/2)$ 110 partial dislocations plus APB” configurations [Figure 7: see original paper].

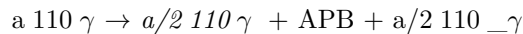
During creep, $a/2$ 110 dislocations in the γ matrix move to γ/γ interfaces, pile up, and shear into γ due to stress concentration. With low stacking fault energy in γ at 760 °C, the $a/2$ 110 dislocation decomposes on $\{111\}$ into two partials: a leading $a/3$ 112 superlattice Shockley partial entering γ and a trailing $a/6$ 112 Shockley partial remaining at the interface, with an SISF between them on $\{111\}$. This matches the fault configurations observed at 760 °C/760 MPa and 800 °C/650 MPa. The process is illustrated schematically in [Figure 8a: see original paper][24] with the reaction:



Energy analysis suggests reaction (1) is unfavorable. However, at lower temperatures, the coherent γ/γ interface is maintained. When a screw $a/2\ 110$ dislocation shears into γ and decomposes according to reaction (1), the $a/6\ 112$ interfacial partial relieves coherency stresses, lowering system free energy [19]. Thus, “partial dislocations plus stacking fault” configurations form at 760 °C/760 MPa and 800 °C/650 MPa. Compared to 760 °C/760 MPa, fewer stacking faults formed at 800 °C/650 MPa with shorter leading partial penetration [Figure 4a: see original paper], correlating with higher stacking fault energy in γ at 800 °C [24,25]. Lower stacking fault energy facilitates dislocation decomposition and extension, promoting wider fault ribbons [Figure 3: see original paper]. Such “partial dislocations plus stacking fault” configurations resist constriction, suppressing cross-slip and improving creep resistance.

At higher temperatures, increased stacking fault energy [24,25] raises the barrier to dislocation decomposition. Consequently, no “partial dislocations plus stacking fault” configurations were observed at 850 °C/500 MPa [Figure 4b: see original paper]. Two factors explain this: (1) higher temperature increases stacking fault energy, hindering decomposition; and (2) at 850 °C/500 MPa steady-state, γ transformed completely to rafts with interfacial dislocation networks, converting coherent to semi-coherent interfaces and disrupting the energetic conditions for reaction (1).

Although stacking faults were absent at 850 °C/500 MPa, “ $a/2\ 110$ partial dislocations plus APB” configurations formed [FIGURE:7, dislocation J]. Shearing superdislocations decomposed into two $a/2\ 110$ partials bounding an APB, as illustrated in [Figure 8b: see original paper]:



At 850 °C/500 MPa, interfacial dislocation networks formed [25] [FIGURE:4b, region V]. Dislocations arriving at these networks can react, altering their movement direction [26], promoting climb, relieving stress concentration, and delaying γ shearing while improving creep resistance [27,28]. With continued creep, increased dislocation pile-up and stress concentration eventually enable dislocation pairs to shear γ along interfaces [7]. Raft formation increases interfacial dislocation networks; sufficient stress concentration can damage these networks, allowing a 110 superdislocations to shear γ and decompose into $a/2\ 110$ partials driven by free energy reduction. Since APB formation on $\{111\}$ requires high energy [29–32], the resulting APB width is narrow [Figure 7d: see original paper].

3.2 Kear-Wilsdorf Locks During Creep

For fcc-structured Ni-based superalloys, the easy-slip close-packed planes are $\{111\}$, where activated dislocations initially glide. However, diffraction analysis reveals shearing dislocations on both $\{111\}$ octahedral and $\{100\}$ cube planes [FIGURE:5 and 6, dislocations B and F]. Studies [33,34] show that during creep, dislocations first glide on $\{111\}$ [FIGURE:9, arrow 1] but can cross-slip to $\{100\}$

[FIGURE:9, arrow 2]. Thus, dislocations B and F on $\{100\}$ planes result from cross-slip from $\{111\}$. Once on $\{100\}$, Kear-Wiltsdorf (K-W) locks form—immobile dislocations with non-planar core structures [31] that suppress slip and cross-slip, enhancing creep resistance. This contributes to the excellent creep resistance at 760 °C/760 MPa and 800 °C/650 MPa.

At 850 °C, no dislocations on $\{100\}$ were observed in γ [Figure 7: see original paper]. Analysis suggests that while K-W locks may form by cross-slip from $\{111\}$ to $\{100\}$ at 850 °C, thermal activation at this higher temperature enables dislocations in K-W locks to cross-slip back to $\{111\}$ [33], releasing the locks and restoring glide on $\{111\}$ [FIGURE:9, arrow 3]. Once released, the non-planar core structure no longer impedes dislocation motion, reducing resistance and degrading creep strength.

Furthermore, the “(a/2) 110 partial dislocations plus APB” configuration formed at 850 °C/500 MPa also suppresses cross-slip [29–32] and improves creep resistance [37], compensating for the absence of stacking faults.

4. Conclusions

1. During steady-state creep of [001]-oriented Ni-based single crystal superalloys at 760 °C/760 MPa and 800 °C/650 MPa, shearing dislocations decompose in γ , where a/3 112 superlattice Shockley partials extend into γ while a/6 112 Shockley partials remain at γ/γ interfaces, with superlattice intrinsic stacking faults (SISF) between them.
2. At 760 °C and 800 °C, a 110 superdislocations shearing into γ can cross-slip from $\{111\}$ to $\{100\}$ planes, forming K-W locks with non-planar core structures. These locks inhibit dislocation slip and cross-slip, contributing significantly to creep resistance.
3. During creep at 850 °C/500 MPa, the deformation mechanism in this higher stacking fault energy regime involves matrix slip and shearing of rafted γ , where a 110 superdislocations decompose into “(a/2) 110 partial dislocations plus APB” configurations. Thermal activation at 850 °C causes dislocations in K-W locks to cross-slip back to $\{111\}$, explaining the disappearance of K-W locks at this temperature.

References

- [1] Tian S G, Zhang S, Liang F S, Li A N, Li J J. Mater Sci Eng, 2011; A528: 4988
- [2] Xia Y F, Jin Y L. J Northeast Univ (Nat Sci), 2008; 29: 1053
- [3] Liu L, Huang T W, Zhang J, Fu H Z. Mater Lett, 2007; 61: 227
- [4] Reed R C, Tao T, Warnken N. Acta Mater, 2009; 57: 5898
- [5] Ma W Y, Li S S, Qiao M, Gong S K, Zheng Y R, Han Y F. Chin J Nonferrous Met, 2006; 16: 937
- [6] Zhang J, Li J G, Jin T, Sun X F, Hu Z Q. Mater Sci Eng, 2010; A527: 3051

- [7] Zhang J X, Murakumo T, Koizumi Y, Kobayashi T, Harada H. Acta Mater, 2003; 51: 5073
- [8] Rae C M F, Matan N, Reed R C. Mater Sci Eng, 2001; A300: 125
- [9] Kear B K, Leverant G R, Oblak J M. Trans ASM, 1969; 62: 639
- [10] Leverant G R, Kear B H. Metall Trans, 1970; 1: 491
- [11] Kear B H, Oblak J M, Giamei A F. Metall Trans, 1970; 1: 2477
- [12] Link T, Feller-Kniepmeier M. Metall Trans, 1992; 23A: 99
- [13] Yu X F, Tian S G, Du H Q, Wang M G, Meng F L. Rare Met Mater Eng, 2007; 36: 2148
- [14] Sass V, Glatzel U, Feller-Kniepmeier M. In: Kissinger R D, Deye D J, Anton D L, Cetel A D, Natal M V, Pollock T M, Woodford D A eds., Superalloys 1996, Warrendale, PA: TMS, 1996: 283
- [15] Sass V, Glatzel U, Feller-Kniepmeier M. Acta Metall Mater, 1996; 44: 1967
- [16] Matan N, Cox D C, Carter P, Rist M A, Rae C M F, Reed R C. Acta Mater, 1999; 47: 1549
- [17] Caron P, Khan T. Mater Sci Eng, 1983; 61: 173
- [18] Lin D L, Lin T L, Wen M. Mater Sci Eng, 1989; A113: 207
- [19] Liu L R, Jin T, Zhao N R, Wang Z H, Sun X F, Guan H R, Hu Z Q. Acta Metall Sin, 2005; 41: 1215
- [20] Tian S G, Ding X, Guo Z G, Xie J, Xue Y C, Shu D L. Mater Sci Eng, 2014; A594: 7
- [21] Yang H, Li Z H, Huang M S. Comput Mater Sci, 2013; 75: 52
- [22] Peng Z F, Ren Y Y, Fan B Z, Yan P, Zhao J C, Wang Y Q, Sun J H. Acta Metall Sin, 1999; 35: 9
- [23] Tian S G, Wu J, Shu D L, Su Y, Yu H C, Qian B J. Mater Sci Eng, 2014; A616: 260
- [24] Milligan W W, Antolovich S D. Metall Trans, 1991; 22A: 2309
- [25] Gabb T P, Draper S L, Hull D R, Mackay R A, Nathal M V. Mater Sci Eng, 1989; A118: 59
- [26] Tian S G, Zhou H H, Zhang J H, Yang H C, Xu Y B, Hu Z Q. Mater Sci Eng, 2000; A279: 160
- [27] Gabrisch H, Mukherji D. Acta Mater, 2000; 48: 3157
- [28] Zhang J X, Murakumo T, Koizumi Y, Kobayashi T, Harada H, Masaki Jr S. Metall Mater Trans, 2003; 33A: 3741
- [29] Doun J, Veyssiere P, Beachamp P. Philos Mag, 1986; 54A: 375
- [30] Veyssiere P, Doun J, Beachamp P. Philos Mag, 1985; 51A: 469
- [31] Foiles S M, Daw M S. J Mater Res, 1987; 2: 5
- [32] Chen S P, Voter A F, Srolovitz D J. Scr Metall, 1986; 20: 1389
- [33] Kear B H, Wilsdorf H G F. Trans Met Soc, 1962; 224: 382
- [34] Liu J L, Jin T, Zhang J H, Hu Z Q. Acta Metall Sin, 2001; 37: 1233
- [35] Vitek V. Prog Mater Sci, 1992; 36(1): 1
- [36] Yamaguchi M, Umakoshi Y. Prog Mater Sci, 1992; 34(1): 1
- [37] Vitek V. Intermetallics, 1998; 6: 579

Note: Figure translations are in progress. See original paper for figures.

Source: ChinaXiv – Machine translation. Verify with original.